



Direct connection of WECS system to the MV grid with multilevel converters

Santiago A. Verne*, María I. Valla

Facultad de Ingeniería, Departamento de Electrotecnia, Universidad Nacional de La Plata and CONICET, Laboratorio de Electrónica Industrial, Control e Instrumentación (LEICI), calle 49 y 118 s/n, La Plata, Bs. As., Argentina

ARTICLE INFO

Article history:

Received 23 December 2010

Accepted 17 November 2011

Available online 10 December 2011

Keywords:

Wind energy conversion system

Current control

Voltage Source multilevel converters

Model predictive control

Variable speed wind turbine

ABSTRACT

A medium voltage power interface for a variable speed Wind Turbine is presented in this paper. The converter topology consists on the Back-to-Back connection of two medium voltage Diode Clamped Multilevel Inverters (DCMI) in the full power path. This mitigates traditional tradeoffs around the low voltage connection between the generator and the grid on the megawatt range. Also, this configuration allows for higher control versatility for grid codes compliance. The converter controllers are based on a Finite-States Model Predictive Control approach, leading to fast dynamic response and DC bus voltage equalization. The control scheme can be used with converters of an arbitrary number of levels with reduced computational effort. This is based on necessary switching restrictions which allow the reliable operation of converter legs. The performance of the control scheme is evaluated through computer simulations.

© 2011 Elsevier Ltd. All rights reserved.

1. Introduction

Increasing energy demands and the perspective of a medium-term shortage of fossil fuels are driving large amounts of research on renewable power technologies. Wind energy systems are one of the most successful technology, not only in academic but also in the industrial field. Through the years, power converters have gained significant prominence because their high control versatility allows them to fulfill the control requirements stated by both the renewable source itself and the grid codes.

In order to increase energy efficiency, variable speed operation of modern Wind Energy Conversion Systems (WECS) has been widely adopted. The demand for sustainable electric power and a lower cost per megawatt is constantly pushing the boundary of WECS to a higher power capacity, thus increasing the rating requirements for all the sub-systems including the tower, machinery and associated power converters. Today, high power wind turbines are ranging from 3 to 7.5 MW [1].

Although modern variable-speed turbines use either Doubly Fed Induction Generators (DFIG) or Field Excited Synchronous Generators, the lower price of permanent magnets is increasing the interest in high power Permanent Magnet Synchronous Generators (PMSG) [2,3]. The PMSG combines low maintenance with a high power-size ratio and gearless transmission capability, enhancing mechanical efficiency and robustness [4].

The Multilevel Converter (MC) is a better choice than the parallel connection of low voltage converters in the megawatt range [5]. Multilevel Converter applications such as motor drives, Active Power Filters and FACTS-based Power Quality solutions can be found in the literature [6,7]. The full-scale Back-to-Back (B2B) converter configuration, jointly with the PMSG, allows higher efficiency and controllability at the generator and grid side when compared with the rectifier-chopper design. It has major advantages regarding grid code compliance with respect to DFIG based solutions, which are limited to approximately 30% of the turbine's rated power.

Locating the coupling transformer in the nacelle also benefits the utilization of Medium Voltage (MV) equipment [8], saving costs especially in offshore wind farms where any additional facility at the bottom is very expensive. However, this is generally avoided due to mechanical loading restrictions on the tower, since the step-up transformer represents about 50 or 70% of the total converter weight [6,9]. Moreover, low voltage machines in the megawatt range must deliver several hundred amperes, causing high copper losses and voltage drop over the connection cables. To overcome this issue, large diameter cables are used with consequent impacts on cost and twisting capability [8]. This design context suggests that the medium voltage migration of high power wind generators is unavoidable. Some works deal with this issue, considering various multilevel converter topologies [10,11,12]. Multipole Synchronous Generators are also considered in [4,13,14], and commercial solutions in this area are available at this time [15,16,17].

* Corresponding author. Tel./fax: +54 0221 4259306.

E-mail address: santiagoverne@gmail.com (S.A. Verne).

Nomenclature

L_C, r_C	Coupling inductor parameters
L_s, R_s	Generator winding parameters
GrC	Grid Converter
GeC	Generator Converter
C_p	Turbine's Power Coefficient
λ	Tip-wind speed ratio
N	Number of converter levels
k	Sampling index
m	Intermediate DC bus node position index
Δ	Step increment in converter leg voltage
g	Generic cost function
K	Generic weighting factor
T_s	Sampling period
ω_t	Turbine rotational speed

V_W	Wind speed
R	Turbine radius
ρ	Air density
V_{ab}, V_{bc}	Line voltages
V_a, V_b, V_c	Phase voltages
ψ_s	Flux linking the stator windings
ψ_m	Flux induced by rotor magnets
θ_r	Generator rotor angle
ω_r	Generator rotational speed
i_d, i_q	Current components in $d-q$ reference frame
P	Number of pole pairs of the generator
K_{gb}	Gear box ratio
T_g	Generator electromagnetic torque
$P_{t,max}$	Available maximum power from the turbine
$T_{t,opt}$	Optimum load torque

This work analyzes the performance of a B2B multilevel converter DCMI which avoids the step up coupling transformer, allowing the high power WECS to be connected directly to the medium voltage grid. Converter control is addressed through the Finite-States Model Predictive Control (FS-MPC) approach, which appears as the natural control strategy to deal with the DC bus voltage balance and presents a fast dynamic response. The proposal is evaluated through computer simulations.

2. System overview

Fig. 1 shows a block diagram of a variable speed turbine comprised of a PMSG and a Back-to-Back DCMI power converter.

The basic control goals for both the Generator Converter (GeC) and the Grid Converter (GrC) are the optimization of the wind power resource and a proper interface with the utility grid, respectively. The GeC controls the machine in order to extract the maximum amount of power from the wind. When normal conditions are present on the grid, the control strategy of the GeC defines the load torque, and thereby the electric power to be extracted, to reach the optimum operation point of the turbine. This power is transferred to the DC link and redirected to the grid at a constant frequency by means of the DC bus voltage control, which is executed by the GrC. Also, when voltage sag occurs, the GrC injects reactive power proportional to the sag amplitude to restore the grid voltage.

3. Converter control

The Back-to-Back DCMI internal structure is shown in Fig. 2. It is composed of two identical Diode Clamped Multilevel Converters with a shared DC bus. Each converter is composed of the clamping diodes, which connect the intermediate DC bus nodes with the converter legs, as well as the active devices with their corresponding free-wheeling diodes.

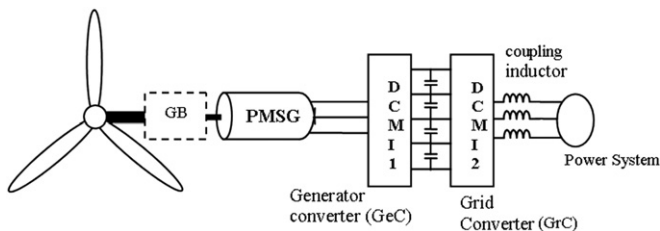


Fig. 1. WECS block diagram.

The goal of the GrC is to regulate the DC bus voltage and control the reactive current when a grid fault occurs. The GeC controls the current in the PMSG to maximize power extraction. These objectives are carried out separately using Model Predictive Control (MPC) strategy. Two key points should be considered to control the internal variables and to comply with the topological constraints of the DCMI [18]. The first deals with the voltage balancing action of the DC bus capacitors and the second with the required switching restrictions over converters legs. The MPC algorithm can provide a control solution for both the external and internal variables. It has been demonstrated in the literature that proper and independent switching sequence selection in B2B connected DCMI is a satisfactory control method to yield reliable converter operation. In particular, MPC strategy has been demonstrated to be an adequate approach to control the current, power, and even induction motors and permanent magnet machines [19].

The indirect voltage clamping of inner devices forces the converter legs to switch one voltage level at a time. This ensures correct blocking voltage sharing and avoids transient over-voltages on the power devices. Additionally, this condition reduces the universe of possible switching states from N^3 to 3^3 , where N is the number of converter levels. Eq. (1) represents the set of leg voltages at instant k in terms of the previous state at $(k-1)$, where m_a, m_b, m_c are the bus node index in which the phase legs a, b and c are connected [18].

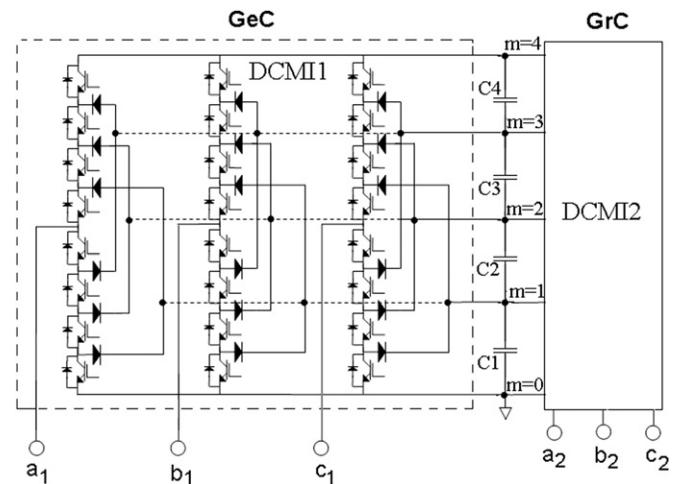


Fig. 2. Back to back DCMI converter circuit.

$$\begin{cases} m_a[k] = m_a[k-1] + \Delta_a & \Delta_a = 0, 1, -1 \text{ and } 0 \leq m_a \leq N-1 \\ m_b[k] = m_b[k-1] + \Delta_b & \Delta_b = 0, 1, -1 \text{ and } 0 \leq m_b \leq N-1 \\ m_c[k] = m_c[k-1] + \Delta_c & \Delta_c = 0, 1, -1 \text{ and } 0 \leq m_c \leq N-1 \end{cases} \quad (1)$$

Given that MPC strategy requires the calculation of every target variable for the universe of possible control actions, an N level DCMI requires $3N^3$ current calculations (three line currents for the N^3 converter states) plus $N^3(N-1)$ capacitor voltages ($(N-1)$ capacitor voltages for N^3 converter states). By virtue of (1), $(N^3 - 3^3)(N+2)$ calculations are saved, which becomes more significant as N increases. The B2B connection with switching sequence control allows the independent execution of both control algorithms. This gives the possibility for parallel computing, optimizing the use of the computational resources.

The core of Model Predictive Control consists of the computation of all target variables, from the present sampling time to the next, using the system dynamic equations. The set of target variables is evaluated for each switching combination to obtain a figure of merit that measures the “distance” between the calculated value and its set point. This calculation is made for each permitted switching combination and a generic global cost function, g , is evaluated for the control vectors. The one that minimizes g is selected for the subsequent sampling period.

$$g = K_1 \cdot g_1 + K_2 \cdot g_2 + K_3 \cdot g_3 + \dots + K_n g_n \quad (2)$$

where g_i and K_i ($i = 1..n$) are the cost functions and their weighting factors, respectively. The weighting factors allow emphasizing the importance of each component in the minimization process [20].

The GeC controller optimizes the working point of the PMSG through torque and reactive current control. Also, voltage balancing control is added by means of a third component. The complete cost function for the GeC is expressed in (3):

$$g_{GeC} = K_{i_q} g_{i_q} + K_{i_d} g_{i_d} + K_{V_{GeC}} g_V \quad (3)$$

where g_{i_q} and g_{i_d} are the cost functions related to the generator currents and g_V is related to the DC bus voltage balance.

The GrC controller stabilizes the DC bus voltage by regulating the power transferred to the grid. It also controls the reactive power to comply with the grid codes in case of a fault or to set the power factor to unity in normal operation. The voltage balance is also considered, leading to the cost function (4):

$$g_{GrC} = K_P g_P + K_Q g_Q + K_{V_{GrC}} g_V \quad (4)$$

Here, g_P and g_Q are the cost functions associated with the active and reactive power injected to the grid, and g_V has the same meaning as before.

3.1. Voltage balance

The B2B topology has been suggested as a method for reaching DC bus voltage balance on Diode Clamped Converters [21]. However, this connection does not self-ensure voltage balance, but also needs a suitable algorithm for redundant switching states selection.

The voltage balance control is based on the forward calculation of capacitors voltages for all potential switching states from one sampling instant to the next using an equivalent circuit model. The analysis presented in [22] allows calculating the capacitor voltage deviations for the possible switching states defined by (1). This is applicable for the generator converter and the grid converter control blocks, independently.

Considering that constant DC bus voltage is forced by the external control loop, the voltage deviation produced at the node in which current is injected, with respect to the negative of the DC bus, is given by (5). The individual capacitor deviation is expressed

in (6). This expression defines the capacitor voltage deviation depending on its location being below or above the node m as indicated in (6) (Fig. 2):

$$\begin{aligned} \Delta V_m &= \frac{T_S I_m(t_0)}{C_{eq-m}} = \frac{T_S I_m(t_0)}{\frac{C}{m} + \frac{C}{N-1-m}} \\ &= \frac{T_S I_m(t_0)}{C} \left(\frac{m(N-1-m)}{N-1} \right) \end{aligned} \quad (5)$$

$$\Delta V_{Cjm} = \begin{cases} \frac{\Delta V_m}{m} & 0 \leq j \leq m \\ -\frac{\Delta V_m}{N-1-m} & m+1 \leq j \leq N-1 \end{cases} \quad (6)$$

Here, C_{eq-m} is the equivalent capacitance between node m and the negative of the DC bus, N is the number of converter levels and T_S is the switching period. The voltage deviation over capacitor j due to the three phase currents i_a , i_b and i_c is:

$$\Delta V_{Cj} = \Delta V_{Cja} + \Delta V_{Cjb} + \Delta V_{Cjc} \quad (7)$$

This expression allows predicting the capacitor voltages for all possible switching combinations. Then, a global cost function that evaluates the DC bus voltage balance through the calculation of capacitor voltage error is defined in (8).

$$g_V = \frac{1}{4} \sum_{i=1}^4 \frac{|V_{Cref} - V_{Ci}|}{V_{Cref}} \quad (8)$$

4. Generator-side converter control

Fig. 3 shows a block diagram of the generator converter and its control scheme. The external control strategy consists of regulating the turbine rotational speed, ω_t , and establishing the tip-speed ratio, λ , at its optimal value, λ_{opt} . This depends on the current wind speed V_W :

$$\lambda_{opt} = \frac{\omega_{t-opt} R}{V_W} \quad (9)$$

When this condition is present, the maximum power that can be extracted, and the corresponding torque are given in (10):

$$P_{t-max} = \frac{1}{2} \rho \pi R^2 V_W^3 C_{Pmax} \quad (10a)$$

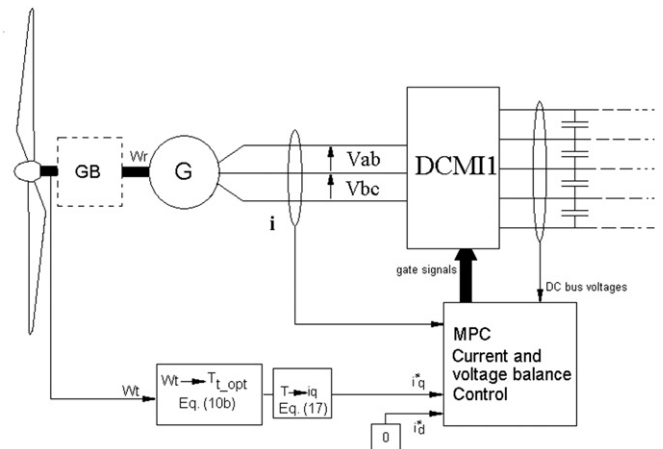


Fig. 3. Block diagram of the generator-side converter control.

$$T_{t_opt} = \frac{1}{2} \rho \pi R^3 \frac{C_{pmax}}{\lambda_{opt}^3} \omega_{t_opt}^2 \quad (10b)$$

where ρ is the air density, R the turbine radius and C_{pmax} the power coefficient at $\lambda = \lambda_{opt}$. The generator converter is devoted to controlling the line currents in order to adjust the torque to its optimal value (10(b)), which is achieved by the proper selection of GeC output voltages. The phase voltages on the motor windings are calculated in terms of converter line voltages through (11):

$$\mathbf{V} = \begin{bmatrix} V_a \\ V_b \\ V_c \end{bmatrix} = \frac{1}{3} \begin{bmatrix} 2 & 1 \\ -1 & 1 \\ -1 & -2 \end{bmatrix} \begin{bmatrix} V_{ab} \\ V_{bc} \end{bmatrix} \quad (11)$$

The PMSG dynamic equation [19] is:

$$\mathbf{V} = R_s \mathbf{i} + \frac{d\psi_s}{dt} \quad (12)$$

where \mathbf{i} is the line current and ψ_s is the flux linking the stator windings that depends on the flux produced by the rotor magnets (ψ_m) and the stator current as represented in (13):

$$\psi_s = L_s \mathbf{i} + \psi_m e^{j\theta_r} \quad (13)$$

Transforming to the d - q rotor reference frame yields (14), where P represents the number of pole pairs of the generator:

$$\begin{cases} \frac{di_d}{dt} = \frac{1}{L_d} V_d - \frac{R}{L_d} i_d + \frac{L_q}{L_d} P \omega_r i_q \\ \frac{di_q}{dt} = \frac{1}{L_q} V_q - \frac{R}{L_q} i_q - \frac{L_d}{L_q} P \omega_r i_d - \frac{\psi_m P \omega_r}{L_q} \end{cases} \quad (14)$$

Performing a forward Euler approximation on Eq. (14) gives:

$$\begin{aligned} i_d[k+1] &= T_s \left(\frac{1}{L_d} V_d[k] - \frac{R}{L_d} i_d[k] + \frac{L_q}{L_d} P \omega_r i_q[k] \right) + i_d[k] \\ i_q[k+1] &= T_s \left(\frac{1}{L_q} V_q[k] - \frac{R}{L_q} i_q[k] - \frac{L_d}{L_q} P \omega_r i_d[k] - \frac{\psi_m P \omega_r}{L_q} \right) + i_q[k] \end{aligned} \quad (15)$$

Both equations are evaluated for all available switching states described by (1). A cost function that measures the "distance" between the reference values and those predicted has the expression (16) for both current components:

$$\begin{aligned} g_{i_d} &= \frac{|i_d[k+1] - i_d^*|}{i_{rated}} \\ g_{i_q} &= \frac{|i_q[k+1] - i_q^*|}{i_{rated}} \end{aligned} \quad (16)$$

where i_d^* and i_q^* are the current references, which have the expressions (17a) and (17b).

$$i_d^* = 0 \quad (17a)$$

$$i_q^* = \frac{2}{3P\psi_m} \frac{T_{t_opt}}{K_{gb}} \quad (17b)$$

The switching state that minimizes (3), taking into account (8) and (16), is selected as the next switching state of the converter.

5. Grid-side converter control

Renewable energy sources connected to the utility grid must comply with operational specifications, especially in regard to grid disturbances. Today, the high penetration of alternative energy

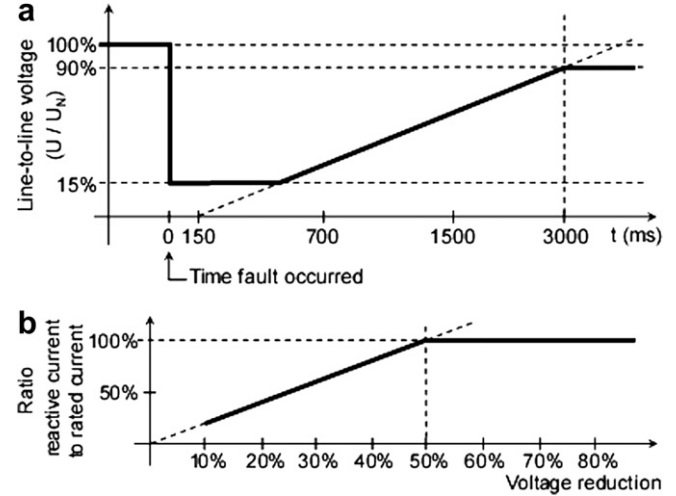


Fig. 4. Grid code requirements: (a) Disconnection restriction, (b) Amount of reactive current to be injected.

sources has motivated grid code enforcement to support the stability of the power system. Regulations apply to the connection holding time when a fault occurs, but also ancillary services like reactive power injection for voltage restoration [23]. Fig. 4(a) shows the disconnection boundary as a function of time depending on the voltage sag magnitude and its duration. Fig. 4(b) shows the amount of reactive current, relative to the system's rated current, depending on the sag amplitude. When reactive power is injected to the grid, active power transfer should be reduced or nullified to avoid exceeding the rated current of the GrC. Then, during the fault, the generator must be de-loaded to avoid the excessive increase of the DC bus voltage. Although this causes turbine acceleration, small speed deviations are produced due to the high value of rotor inertia and the short fault operation times [24,25]. However, if the fault exceeds the time of connection holding, pitch angle control (which is not considered in this study) can prevent over speed [26].

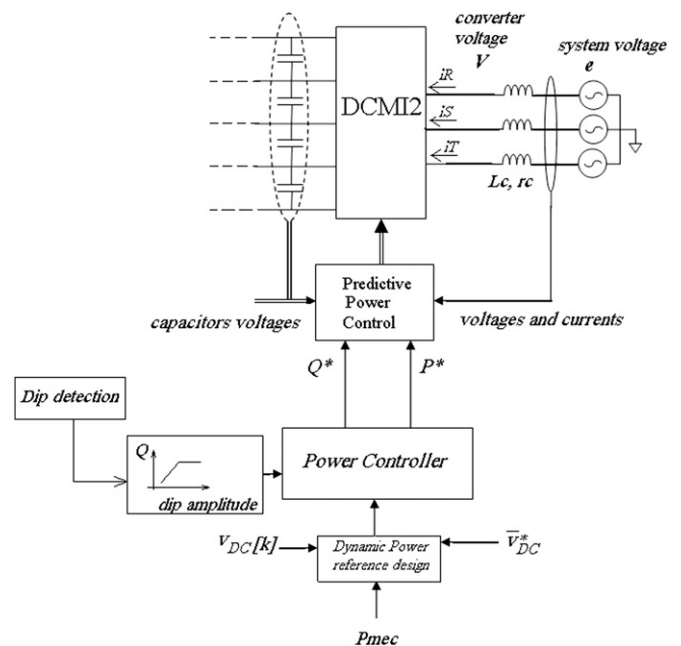


Fig. 5. Grid side converter control diagram.

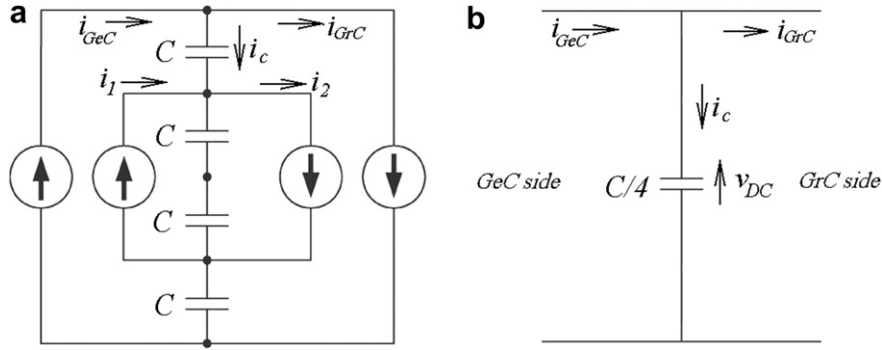


Fig. 6. DC bus equivalent circuit (a) Current flow model, (b) Simplified model for power balance.

5.1. Active and reactive power calculation

Fig. 5 shows a block diagram of the GrC controller whose predictive strategy performs a calculation of real and imaginary power for all the switching combinations. For each of these cases, future values of line currents are calculated. At a given sampling instant k , phase voltages $\mathbf{e}[k]$ and currents $\mathbf{i}[k]$ are sampled. The active and reactive power supplied to the AC system at instant $(k+1)$ can be calculated applying the Instantaneous Power Theory, through a prediction of the line currents. This calculation is performed by evaluating (18), where the system voltage \mathbf{e} is considered to be constant along T_s ($\mathbf{e}[k+1] \approx \mathbf{e}[k]$) [4].

$$\begin{bmatrix} i_a \\ i_b \\ i_c \end{bmatrix}_{K+1} = \frac{T_s}{3L_c} \left(\begin{bmatrix} -2 & -1 \\ 1 & -1 \\ 1 & 2 \end{bmatrix} \left(\begin{bmatrix} V_{ab} \\ V_{bc} \end{bmatrix}_K - \begin{bmatrix} e_{ab} \\ e_{bc} \end{bmatrix}_K \right) \right) + \left(1 - \frac{r_c T_s}{L_c} \right) \begin{bmatrix} i_a \\ i_b \\ i_c \end{bmatrix}_K \quad (18)$$

where T_s is the sampling period, r_c the coupling inductor resistance and e_{xy} , V_{xy} the line voltages at the power system and the converter sides, respectively. Using the stationary transformation and following the switching constraint defined in (1), active and reactive power supplied by the AC system can be calculated with expression (19). At most, a set of 27 values of active and reactive power, corresponding to the possible converter switching states are calculated.

$$\begin{aligned} P[k+1] &= e_\alpha[k]i_\alpha[k+1] + e_\beta[k]i_\beta[k+1] \\ Q[k+1] &= e_\beta[k]i_\alpha[k+1] - e_\alpha[k]i_\beta[k+1] \end{aligned} \quad (19)$$

The optimization functions associated with P and Q are designed to indicate how far the power predicted by (19) is from the reference value. Individual cost functions are defined in (20) for P and Q , normalized to the rated power of the converter:

$$\begin{aligned} g_P &= \left| \frac{P[k+1] - P^*[k+1]}{P_{rated}} \right| \\ g_Q &= \left| \frac{Q[k+1] - Q^*[k+1]}{P_{rated}} \right| \end{aligned} \quad (20)$$

The reference value Q^* of reactive power is set depending on the power mode as described before (normal or fault mode). The dynamic active power reference P^* is shaped using the equations of power balance taking into account the measured power at the output of GrC and the energy storage per unit time of the DC bus.

In normal operation, the control target of the GrC is the voltage regulation of the DC link. This is necessary given that the power which is injected to the DC bus by the GeC tends to increase this voltage. Also, in normal grid conditions it is desirable to present a high power factor to the utility grid. The GrC controller also takes into account the balancing of the capacitors by selecting the best switching combinations in order to minimize the cost function.

The DC bus voltage control works by predicting the power balance between the incoming and outgoing power and the stored energy in the DC bus. A Dynamic Power Reference Design block makes this calculation [27]. For a five level DCM, an equivalent circuit of the DC bus is illustrated in Fig. 6 [28].

Considering the operation in voltage balance condition yields $i_1 = i_2$. Then, it follows that the current flowing through all capacitors has the same value i_c . Fig. 6(a) can be simplified to 6(b) where the equivalent capacitance C_{dc} equals $C/4$.

The active power reference signal, P^* , is the sum of a feedforward term, which depends on the power delivered to the load, and a correction term that measures the necessary power to re-establish the DC bus voltage to its reference value.

The DC load current i_{GrC} is determined by a rotor speed measurement and an electromagnetic torque estimation:

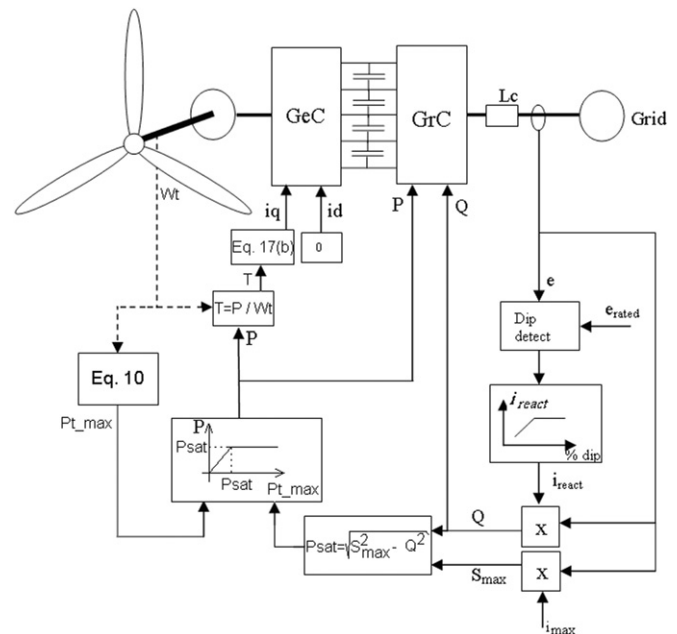


Fig. 7. Power control block diagram.

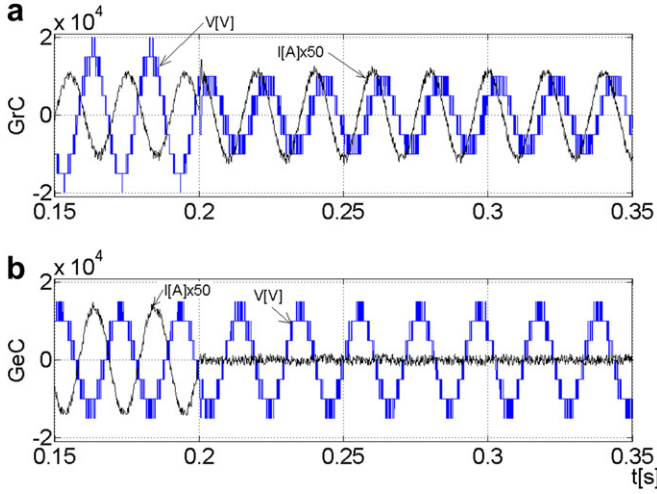


Fig. 8. Voltages at the dip event (a) GrC voltage and current, (b) GeC voltage and current.

$$i_{GeC} = \frac{P_{mec}}{V_{DC}} \text{ where } P_{mec} = T_g \omega_r \quad (21)$$

The power delivered to the DC bus can be expressed as the energy derivative:

$$P_{DC} \approx \frac{\Delta E_{DC}}{T_s} = \frac{C}{4T_s} v_{DC}[k] (v_{DC}^* - v_{DC}[k]) \quad (22)$$

In order to diminish the control effort, v_{DC}^* is replaced by the average between the present and the reference value.

Finally, the necessary power to be injected to the DC bus by the GeC is P^* given by:

$$P^*[k+1] = P_{mec} + \frac{C}{4T_s} v_{DC}[k] (\overline{v_{DC}^*} - v_{DC}[k]) \quad (23)$$

On the other hand, setting the reactive power reference Q^* depends on the operating mode of the GrC. If the grid voltage is within the 10% band, it is set to zero. If fault mode is present, it is set to a value that depends on the grid codes execution rule.

The complete cost function for the grid converter defined in (4) is evaluated for all available switching states and the switching combination that minimizes this expression is selected as the next state of the GrC.

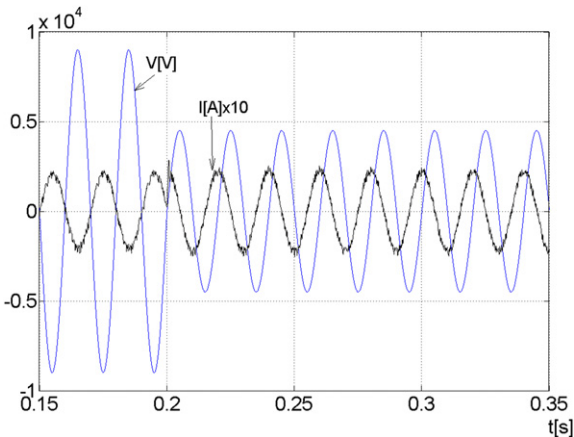


Fig. 9. Grid phase voltage and its corresponding current.

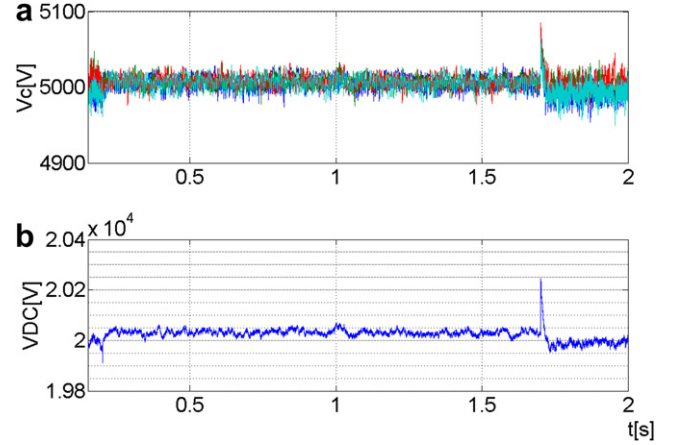


Fig. 10. (a) Capacitor voltages, (b) DC link voltage.

6. Performance evaluation

The control strategy was applied on a 3 MW wind turbine in a Matlab-Simulink environment. The control algorithms were programmed in embedded discrete-time sub-systems and, due to the lack of a predefined DCMI model, the power conversion stage was designed entirely from available discrete components of the Power System Block set.

The system performance was evaluated in both normal and fault mode, in order to analyze the behaviour of the electrical and mechanical variables. The DC bus was set at 20 kV for direct connection to the medium voltage grid, with 1500 μ F capacitors and a grid coupling inductor $L_c = 10$ mH [29]. The sampling frequency was set to 6 kHz, and the equivalent moment of inertia was $J = 10e6$ kgm² [30].

The power controller drives the GrC's predictive algorithm, depending on the grid status. When normal voltage is present ($U_N \pm 10\%$), wind power is supplied to the DC bus by the GeC and injected to the grid by the GrC with a unity power factor. If a fault occurs, a proportional reactive current is provided, yielding a 100% current capacity (up to the maximum current limit, i_{max}) for 50% sag amplitude, as stated in Fig. 4. The active power transfer is decreased as reactive current demand increases in order to prevent exceeding the converter's current limit. This gives a partial braking capability of the rotor during fault events. A block diagram is shown in Fig. 7.

First, the operation is set just below the rated wind speed (11.8 m/s) with an output power of 2.9 MW. At $t = 0.2$ s, a 50%

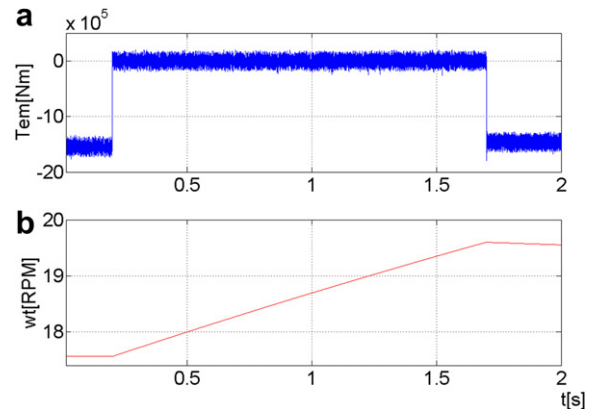


Fig. 11. Mechanical variables, (a) Generator torque, (b) Turbine speed.

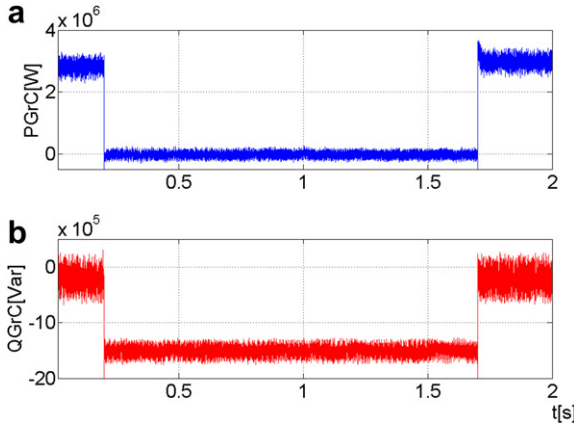


Fig. 12. (a) Active power injected to the grid by GrC, (b) Reactive power consumed from the grid.

voltage dip is introduced. Based on Fig. 4, 100% of the converter's rated current has to be injected with a pure reactive power factor in order to contribute to grid voltage restoration. In this condition the conversion system has to be able to handle this condition for at least 1.5 s (Fig. 4) and return to normal condition after the fault.

Fig. 8 shows the corresponding voltages and currents at both converters' AC terminals. Fig. 8(a) shows a GrC AC line voltage and current around the fault region, while Fig. 8(b) shows the line voltage and current at the GeC terminals. It can be seen that the corresponding phase shift in both graphs is near 30° . For better visualization, both currents are amplified by 50. The number of voltage levels used in the GrC, during the dip, is reduced in order to reach the desired reactive current value. Fig. 8(b) depicts the complete generator de-loading during the fault. Fig. 9 shows one grid phase voltage and the corresponding current during this event and demonstrates that the required current phase shift for grid code fulfilment is rapidly reached from pure active to pure reactive.

The capacitor voltages and DC bus voltage are shown in Fig. 10a and b, respectively. Even in the presence of the grid disturbance, the capacitor voltages remain stable and balanced with a maximum deviation of less than 2%, while the DC bus suffers a small deviation of approximately 1% from its reference value. In stationary rated active power transfer conditions, the capacitor voltages present a ripple of 80Vpp, which is 1.6% in respect to their reference values. During the sag, the ripple reduces to 50Vpp which represents only 1% of the rated value.

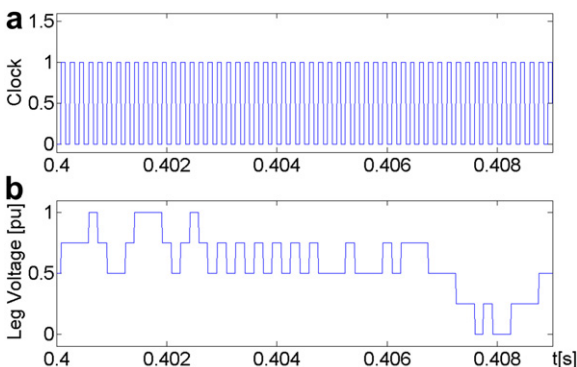


Fig. 13. (a) Clock signal for MPC execution, (b) Converter leg voltage normalized to V_{DC} .

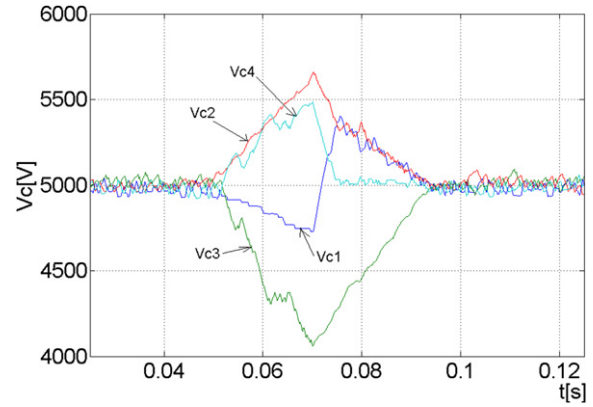


Fig. 14. DC capacitor voltages while $K_{VGeC} = 0$.

The mechanical variables of the generator are shown in Fig. 11. The EM torque is shown in 11(a) and the turbine speed in 11(b). Acceleration is observed within the dip occurrence, but it is not significant due to the high value of rotor inertia. Excess stored energy is evacuated after grid restoration with the speed limit given by the GrC's rated current capacity. This is represented in Fig. 11(b) through the negative slope of the turbine speed after $t = 1.7$ s

The active and reactive powers are measured at the grid side and are shown in Fig. 12. It is observed that within the fault time, the active power transfer is almost cancelled due to the complete de-loading of the generator. The reduction of load torque reflects the rotor acceleration shown in Fig. 11(b). A fast dynamic response of reactive power injection is observed in Fig. 12(b). Given that the power system dip amplitude is 50%, the maximum apparent power, S_{max} (Fig. 7), is one half of the converter's rated power (3 MW). This is seen in Fig. 12(b) as 1.5MVar of reactive power injected to the grid.

The sampling clock and one normalized leg voltage are shown in Fig. 13. Only one voltage level transition is observed at all times, fulfilling the constraint given in (1).

The effectiveness of voltage balance strategy by including the associated cost function components g_V and their weighting factors K_{VGeC} and K_{VGRC} is also explored. An additional test showing the counteracting synergic effect of the Back-to-Back connection for DC bus voltage balance is performed. In order to verify the incidence of voltage balance components in the GrC and GeC cost functions, both weighting factor values K_{VGeC} and K_{VGRC} are changed from their normal value to zero. This implies, according to (3), (4) and the cost function minimization exposed in Section 3, that no importance is

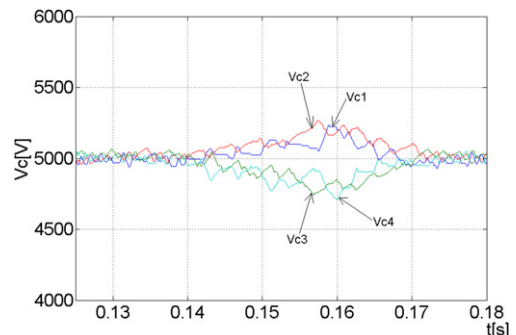


Fig. 15. DC capacitor voltages while $K_{VGRC} = 0$.

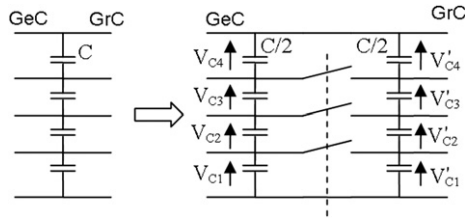


Fig. 16. Disconnection of intermediate nodes.

assigned to voltage balance for switching states selection. Initially, the system is almost at the rated power generation level (2.9 MW). From $t = 0.05$ s to $t = 0.07$ s $K_{V_{GeC}}$ is changed from its normal value of 0.1 to 0, such that no feedback for voltage balance applies for the GeC. It is observed from Fig. 14 that capacitor voltages start to diverge from their set point values until $K_{V_{GeC}}$ is restored, when they immediately start to return to their original values. Similarly, Fig. 15 shows the results of the same operation on $K_{V_{GrC}}$ from $t = 0.14$ s to $t = 0.16$ s. As before, voltage unbalance begins, but it is corrected when feedback is restored. The difference in the rate of change of capacitor voltages (Figs. 14 and 15) is related to the difference in modulation indexes of the GrC and GeC. While GrC operates with a modulation index near unity (see line voltage waveforms of Fig. 8 from $t = 0.15$ s to $t = 0.2$ s), the GeC operates with a lower one. This implies that more redundant states are available and a stronger balancing action can be performed by the GeC than the GrC. Also, when both converters are enabled to contribute, capacitor voltages naturally remain at their reference values.

Finally, the balancing effect of the B2B connection is shown by disconnecting the intermediate DC bus nodes while maintaining $K_{V_{GrC}}$ and $K_{V_{GeC}}$ at normal values. DC capacitors were split at both sides of the converters and a small resistance switch was inserted between them as indicated in Fig. 16.

First, the switch is closed and voltage balance is achieved (normal operation). The switches are opened at $t = 0.3$ s and reclosed again at $t = 0.32$ s. It can be observed in Fig. 17 that voltage unbalance begins immediately, but it is rapidly solved after switch reclosing, proving the compensation effect between both converters. Also, inner capacitors show the antagonistic charge/discharge characteristics from both the GrC and GeC sides. Capacitors C_2 and C_3 discharge at the GrC side, which is the typical pattern for DC to AC power flow, while the opposite occurs for their counterparts on the GeC side (AC to DC power flow). Of course, as the DC bus voltage was maintained constant by the GrC active power control loop, the contrary effect was also experienced by C_3 and C_4 on both sides of the DC bus.

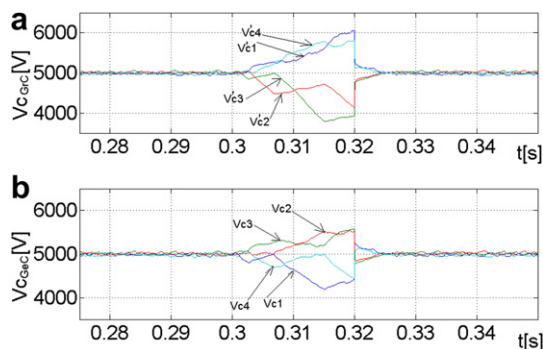


Fig. 17. Unbalancing effect of DC bus capacitors due to temporary disconnection of intermediate nodes, (a) GrC-side capacitors, (b) GeC-side capacitors.

7. Conclusions

A transformerless WECS interface has major advantages when compared with traditional low voltage converters. It is demonstrated that the multilevel power interface performs well regarding the main control objectives and also presents reliable potential to perform ancillary services required by the grid operator. A satisfactory assessment is made with respect to the control of power converters and their internal variables by means of the Model Predictive Control strategy. The fact that both converters can execute their control routines in an autonomous way gives significant alleviation of computational constraints through the parallel execution of both control routines.

Acknowledgments

This work was supported by Universidad Nacional de La Plata (UNLP), CONICET and ANPCyT.

References

- [1] "E-126 7.5MW turbine", ENERCON magazine for wind energy. No. 4, <http://www.enercon.de>; 2007.
- [2] Chen Z, Guerrero J, Blaabjerg F. A review of the state of the art of power electronics for wind turbines. *IEEE Trans. Power Electronics* 2009;24:1859–75.
- [3] Carrasco JM, Franquelo LG, Bialasiewicz JT, Galvan E, Guisado RCP, Prats MM, et al. Power-electronic systems for the grid integration of renewable energy sources: a survey. *IEEE Trans Ind Electronics* 2006;53:1002–16.
- [4] Winkelkemper M, Wildner F, Steimer P. Control of a 6 MVA hybrid converter for a permanent magnet synchronous generator for windpower. *Proc of the 18th Int. Conf Electrical Machines (ICEM '2008)*; 2008:1–6.
- [5] Kouro S, Malinowski M, Gopakumar K, Pou J, Franquelo LG, Wu B, et al. Recent advances and industrial applications of multilevel converters. *IEEE Trans. Ind Electr* 2010;57:2553–80.
- [6] Abu-Rub H, Holtz J, Rodriguez J, Baoming G. Medium voltage multilevel converters- State of the art, challenges, and requirements in industrial applications. *IEEE Trans. Ind Electr* 2010;57:2581–95.
- [7] Rodriguez J, Bernet S, Wu B, Pontt J, Samir Kouro. multilevel voltage source converter topologies for industrial medium-voltage drives. *IEEE Trans. Ind Electr* 2007;54:2930–45.
- [8] Chong H Ng, Parker MA, Ran L, Tavner PJ, Bumby JR, Spooner E. A multilevel modular converter for a large, light weight wind turbine generator. *IEEE Trans. Power Electronics* 2008;23:1062–74.
- [9] Akagi H. The next-generation medium-voltage power conversion systems. *J Chin Inst Engineers* 2007;30:1117–35.
- [10] Li J, Zhu Y, Xu Hgyan, Xu Honghua. CPS-SPWM flying capacitor three-level back-to-back converter applicative direct-drive wind power generator system. *Proc. Of the International Conference on sustainable power generation and Supply (SUPERGEN '09)*; 2009. pp. 1–6.
- [11] Yuan X, Li Y, Chai J. A transformerless modular permanent magnet wind generator system with minimum generator coils. *Twenty-Fifth Annual IEEE applied power Electronics Conference and Exposition (APEC2010)*; 2010. pp. 2104–2110.
- [12] Melicio R, Mendes VMF, Catalão JPS. Power converter topologies for wind energy conversion systems: integrated modelling, control strategy and performance simulation. *Renewable Energy* 2010;35:2165–74.
- [13] Fernandez LM, Garcia CA, Jurado F. Operating capability as a PQ/PV node of a direct-drive wind turbine based on a permanent magnet synchronous generator. *Renewable Energy* 2010;35:1308–18.
- [14] Abbes M, Belhadji J, Abdelghani Bennani AB. Design and control of a direct drive wind turbine equipped with multilevel converters. *Renewable Energy* 2010;35:936–45.
- [15] Faulstich A, Stinke JK, Wittwer F. Medium voltage converter for permanent magnet wind power generators up to 5 MW. *Proc. of the European Conference on Power Electronics and Applications (EPE'2005)*; 2005. pp. 1–9.
- [16] Kieferndorf F, Basler M, Serpa LA, Fabian JH, Coccia A, Scheuer GA. A new medium voltage drive system based on ANPC-5L technology. *IEEE International Conference on industrial technology (ICIT'2010)*; 2010. pp. 643–649.
- [17] PCS-6000, 6 MW wind power converter from ABB. <http://www05.abb.com/>.
- [18] Verne SA, Valla MI. Active power filter for medium voltage networks with predictive current control. *Electric Power Syst Res* 2010;80:1543–51.
- [19] Fuentes E, Rodriguez J, Silva C, Diaz S, Quevedo DE. Speed control of a permanent magnet synchronous motor using predictive current control. *IEEE 6th International power Electronics and Motion control Conference (IPEMC '09)*; 2009. pp. 390–395.
- [20] Cortés P, Kouro S, La Roca B, León JI, Vásquez S, Franquelo LG. Guidelines for weighting factors adjustment in finite states model predictive control of power converters and drives. *IEEE International Conference Industrial Technology (ICIT '09)*; 2009. 1–7.

- [21] Lai JS, Peng FZ. Multilevel converters- a new breed of power converters. *IEEE Trans Ind Appl* 1996;32:509–17.
- [22] Verne SA, González SA, Valla MI. An optimization algorithm for capacitor voltage balance of N-level diode clamped inverters. 34th Annual Int. Conf. Of the IEEE Industrial Electronics Soc (IECON'08); 2008. pp. 3201–3206.
- [23] Alepuz S, Busquets-Monge S, Bordonau J, Cortés P, Kouro S. Control methods for low voltage ride-through compliance in grid-connected NPC converter based wind power systems using predictive control. *Energy Conversion Congress and Exposition (ECCE'2009)*; 2009:363–9.
- [24] Ramtharan G, Arulampalam A, Ekanayake JB, Hughes FM, Jenkins N. Fault Ride-through of fully rated converter wind turbines with AC and DC transmission systems. *IET Renewable Power Generation* 2009;3:426–38.
- [25] Rawn B, Lehn P. Rotor Inertia Wind, Efficiency Variable. Fundamental limits on their exploitation for inertial response and power system damping. *Eur Wind Energy Conf (EWEC'08)*; 2008.
- [26] Muljadi E, Butterfield CP. Pitch-controlled variable-speed wind turbine generation. *IEEE Trans. Ind Appl* 2001;37:240–6.
- [27] Quevedo DE, Aguilera RP, Perez MA, Cortes P. Finite control set MPC of an AFE rectifier with dynamic references. *Intl Conf Ind Techn (ICIT'2010)*; 2010:1265–70.
- [28] Pan Z, Peng FZ, Corzine K, Stefanovic V, Leuthen JM, Gataric S. Voltage balancing control of diode-clamped multilevel/inverter systems. *IEEE Trans. Ind Appl* 2005;41:1698–706.
- [29] Portillo RC, Prats MM, Leon JI, Sanchez JA, Carrasco JM, Galvan E, et al. Modeling strategy for back-to-back three-level converters applied to high-power wind turbines. *IEEE Trans. Ind Electronics* 2006;53:1483–91.
- [30] Park Joon-Young, Lee Jae-Kyung, Oh Ki-Yong, Lee Jun-Shin, Kim Beom-Joo. Design of simulator for 3 MW wind turbine and its condition monitoring system. *International MultiConference of Engineers and Computer Scientists (IMECS'2010)* 2010;2.